NORSAR ROYAL NORWEGIAN COUNCIL FOR SCIENTIFIC AND INDUSTRIAL RESEARCH

Scientific Report No. 2-73/74

NORSAR LOCATION CALIBRATIONS AND TIME DELAY CORRECTIONS

by
K. A. Berteussen

Kjeller, 13 January 1974

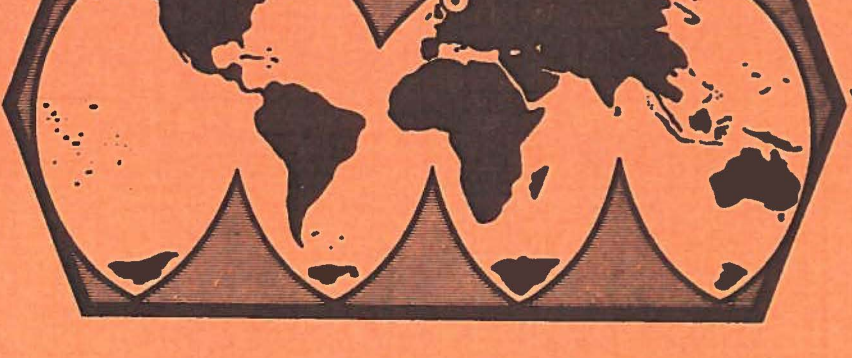

SECURITY CLASSIFICATION OF THIS PAGE (*When Data Entered*)

REPORT DOCUMENTATION PAGE

READ INSTRUCTIONS BEFORE COMPLETING FORM

1. REPORT NUMBER: F44620-74-C-0001	2. GOVT ACCESSION NO. / 3. RECIPIENT'S CATALOG NUMBER
4. TITLE (*and Subtitle*): NORSAR Location Calibrations and Time Delay Corrections	5. TYPE OF REPORT & PERIOD COVERED: Scientific Report
	6. PERFORMING ORG. REPORT NUMBER: Scientific Rep. 2-73/74
7. AUTHOR(s): K.A. Berteussen	8. CONTRACT OR GRANT NUMBER(s): F44620-74-C-0001
9. PERFORMING ORGANIZATION NAME AND ADDRESS: NTNF/NORSAR, Post Box 51, N-2007 Kjeller, Norway	10. PROGRAM ELEMENT, PROJECT, TASK AREA & WORK UNIT NUMBERS: NORSAR Phase 3
11. CONTROLLING OFFICE NAME AND ADDRESS: Air Force Office of Scientific Research, 1400 Wilson Blvd, Arlington, Virginia 22209 U.S.A.	12. REPORT DATE: 3 January 1974
	13. NUMBER OF PAGES: 45
14. MONITORING AGENCY NAME & ADDRESS(*if different from Controlling Office*): European Office of Aerospace Research and Development, Keysign House, 429 Oxford Street, London W1, England Attn: Maj.Munzlinger	15. SECURITY CLASS. (*of this report*)
	15a. DECLASSIFICATION/DOWNGRADING SCHEDULE

16. DISTRIBUTION STATEMENT (*of this Report*)

Approved for public release; distribution unlimited.

17. DISTRIBUTION STATEMENT (*of the abstract entered in Block 20, if different from Report*)

18. SUPPLEMENTARY NOTES

19. KEY WORDS (*Continue on reverse side if necessary and identify by block number*)

Location calibrations, time delay corrections, crustal structure, least squares interface.

20. ABSTRACT (*Continue on reverse side if necessary and identify by block number*)

Deviations from theoretical expected values are observed both for slowness and travel time for P-signals crossing the array. These observed anomalies are presented. At NORSAR these are corrected for both when performing beamforming and when locating events. The method used is explained and the effect of these corrections both on signal detectability and event location is shown to be quite profound. Some simple crust models, plane dipping Moho and a Moho which is a curved interface, are tested and found to be able to explain as a maximum 25% of the observed squared deviations.

DD FORM 1 JAN 73 1473 EDITION OF 1 NOV 65 IS OBSOLETE

SECURITY CLASSIFICATION OF THIS PAGE (*When Data Entered*)

USAF Project Authorization No.	:	VT/4702/B/OSR
Date of Contract	:	30 August 1973
Amount of Contract	:	$ 888,806.00
Contract Termination Date	:	30 June 1974
Project Supervisor	:	Robert Major, NTNF
Project Manager	:	Nils Marås
Title of Contract	:	Norwegian Seismic Array (NORSAR)

CONTENTS

NORSAR LOCATION CALIBRATIONS AND TIME DELAY CORRECTIONS

by

K.A. Berteussen

ABSTRACT

Deviations from theoretical expected values are observed both for slowness and travel time for P-signals crossing the array. These observed anomalies are presented. At NORSAR these are corrected for both when performing beamforming and when locating events. The method used is explained and the effect of these corrections both on signal detectability and event location is shown to be quite profound. Some simple crust models, i.e., plane dipping Moho and a Moho which is a curved interface, are tested and found to be able to explain at most 25 per cent of the observed squared deviations.

1 INTRODUCTION

It is well known that the observed time delays for signals crossing a seismic array exhibit considerable deviations from the theoretically expected values. Especially in case of the LASA array (Large Aperture Seismic Array, Montana, USA) several studies have been made of slowness and travel time anomalies for the purpose of determining the local structure, as well as inhomogeneities in the lower mantle, f. ex., Greenfield and Sheppard (1969), Glover and Alexander (1969), Chinnery and Toksöz (1967), Zengeni (1970), Iyer (1971), Iyer and Healy (1972), Engdahl and Felix (1971), Davies and Sheppard (1972). Also for other arrays there have been similar analyses, f. ex., Niazi (1966), Otsuka (1966), Otsuka (1966a), Johnson (1967), Johnson (1969), Corbishly (1970), Husebye et al (1971). At NORSAR few studies of this type have been made so far - Noponen (1971) and Gjøystdal et al (1973). All the above-mentioned studies have been concerned with what may be termed, loosely speaking, the average or deterministic part of the crustal structure and upper mantle beneath the array. There is, however, a large amount of scatter in the data, which so far seems to be investigated in detail by very few authors: Mack (1969), Aki (1973), Capon (1974) and Dahle et al (1974).

The objective of this report is to present the P-wave slowness and travel time anomalies observed at NORSAR and to explain how these are corrected for (Chapter 2 and 3). The effect of these corrections is presented in the form of measurements of gain in signal detectability and in event location capability (Chapter 4). Some tests will be made whether or not the observed anomalies can be explained by conventional crust models (plane dipping Moho (Chapter 3) or a Moho which is a curved interface (Chapter 5)).

2 DEFINITIONS

2.1 NORSAR Location Calibrations

Let the observed slowness components for a recorded event be UXO and UYO. The corresponding theoretical components, denoted UXC and UYC are calculated from the NOAA epi-center solution using a smoothed version of Herrin's (1968) travel time tables. (The UX-axis points west, while the UY-axis points south.)

The calibration components for the point UXO, UYO in slowness space are then

$$\begin{aligned} DUX &= UXC-UXO \\ DUX &= UYC-UYO \qquad (2.1) \end{aligned}$$

After having observed the components UX,UY, the corrections (DUX,DUY) should thus be added in order to get the components (UXC,UYC) corresponding to the correct solution. (See appendix for program guide.)

2.2 NORSAR Time Delay Corrections

The slowness components (UXO,UYO) discussed in section 2.1 are calculated by least squares fitting of a plane wavefront to a set of time delays measured on the subarray beams. These are denoted D(I), (I=1,NSUB), where NSUB is the number of subarrays. (Corrections within subarrays are not considered in the current system.) These observed delays do not fit exactly to a plane wavefront. Let DPWF(I), (I=1,NSUB), be the set of delays corresponding to the plane wavefront. The region corrections for the point UXO,UYO in slowness space are then given by the following equation:

$$\mathrm{DEV(I)} = \mathrm{DPWF(I)-D(I)} \qquad \mathrm{I=1,NSUB} \qquad (2.2)$$

If the problem is to form a beam aimed at the point UX,UY, this can be done by applying the following subarray delays

$$\mathrm{D(I)} = \mathrm{DPWF(I)-DEV(I)} \qquad \mathrm{I=1,NSUB} \qquad (2.3)$$

where DPWF is calculated as follows:

$$\mathrm{DPWF(I)} = -(\mathrm{X(I)\cdot UX+Y(I)\cdot UY})$$

$$= (\mathrm{X(I)\cdot \sin(AZ)+Y(I)\cdot \cos(AZ))\cdot U} \qquad (2.4)$$

$$\mathrm{I=1,NSUB}$$

X(I), Y(I) are east/west and north/south coordinates respectively (km) for subarray I. AZ is direction of approach (azimuth) for the plane wavefront and U is slowness.

One should note that the DEV(I) definition in eq. 2.2 also includes deviations caused by elevation differences, i.e., the DEV(I) parameter may be considered as a sum of two independent factors

$$DEV(I) = D_{INH}(I) + D_{ELV}(I) \tag{2.5}$$

$D_{INH}(I)$ is the part of the deviation which is caused by real inhomogeneities in the earth. $D_{ELV}(I)$ is the part of the deviation which occurs because the instruments do not have the same elevation. If the P-velocity in the crust under NORSAR is assumed to be V_C and Z(I) is the elevation difference between subarray I and the reference plane, $D_{ELV}(I)$ may be calculated as follows.

$$D_{ELV}(I) = Z(I)\cdot\left(\frac{1}{V_C^{\,2}} - \frac{\sin^2 i_C}{V_C^{\,2}}\right)^{\frac{1}{2}} = Z(I)\cdot\left(U_C^{\,2}-U^2\right)^{\frac{1}{2}} \tag{2.6}$$

3 DATA

3.1 Construction of Data Base

The data base of regional time delay corrections and location calibrations is built up by covering slowness space with a set of triangles. The vertices, or nodes, of these triangles are real data points, and associated with each there are regional correction and calibration data. The regional corrections and calibrations for a certain point in slowness space are then predicted by barocentric interpolation from the values at the vertices (nodes) of the triangle in which the point is situated. For each node there are thus 24 data values, 22 region corrections (one for each subarray) and 2 calibration values (for the UX and UY direction respectively). The set of nodes and their connections are denoted the region correction data base (IBM, 1972).

Fig. 3.1 shows the node points of the current data base (implemented 30 Nov 72) plotted in slowness space. Each node point is based on the observations for one event or it may be constructed by averaging the deviations for several events. The events used for each node, and the corresponding phase are listed in Table 3.1. The delays are calculated by using an iterative cross-correlation procedure (Bungum and Husebye (1971)) after having applied a 1.0-3.0 Hz bandpass (third order recursive Butterworth) filter in order to ensure good signal-to-noise ratio. For some of the events with node numbers less than 52, a 0.8-2.5 Hz bandpass filter has been used. The difference between these two filters is however not believed to be significant in this context (Bungum and Husebye (1971)). It should be noted that for certain areas in slowness space the corrections and calibrations will be interpolations between node points which are based on different phases. According to Engdahl and Felix (1971) the anomalies are found to vary continuously from one phase to another at the LASA array. For example, node 60 is based on PKP observations, while node 99 and 44 are based on P-observations. Inside the triangle 88-99-44 the interpolated values will thus be based on both PKP and P observations.

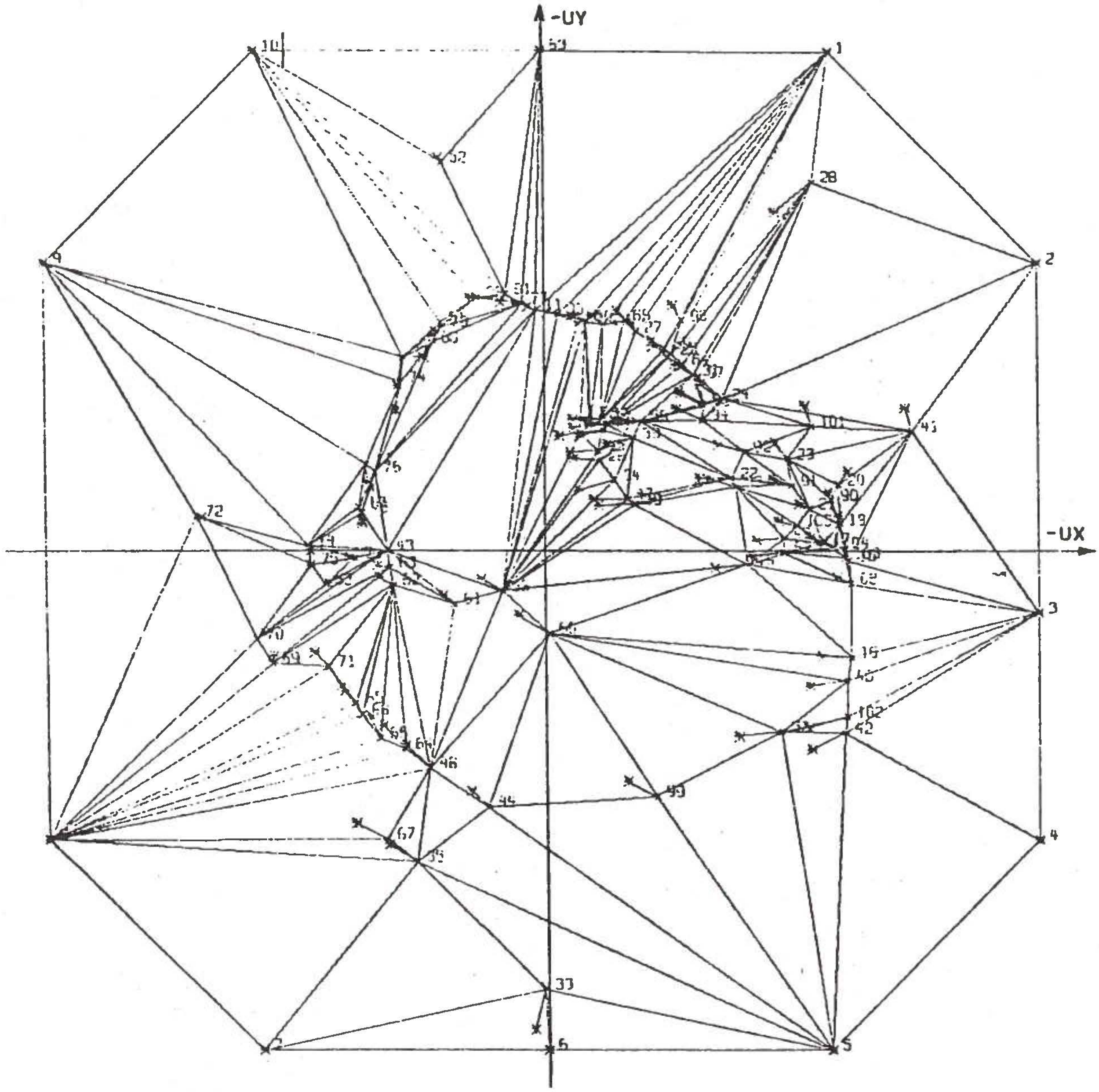

Fig. 3.1 Location calibration vectors as implemented 30 November 72, plotted in slowness space. For each node the observed (node number) and corrected value (star) are indicated.

Node	Event Date	Region	Lat	Lon	m_b	Phase	Dist	Azi
11	09/04/71	Unimak Island Region	55.0N	163.4W	5.8	P	64.3	356.3
12	05/14/71	Chipas, Mexico	16.2N	94.0W	4.8	P	83.0	290.8
13	06/05/71	Costa Rica	9.3N	84.2W	5.4	P	84.0	279.1
14	06/27/71	Mona Passage	19.1N	67.9W	4.9	P	68.0	270.0
15	07/24/71	Todzhik-Sinkiang Border	39.5N	73.2E	5.6	P	42.2	90.1
16	06/26/71	Soutwest Sumatra	5.3S	96.9E	5.8	P	92.7	95.8
17	05/03/71	Tibet	30.8N	84.5E	5.4	P	55.7	87.2
18	07/24/71	Iran	30.4N	59.9E	5.0	P	44.2	110.6
19	07/03/71	Kirgiz-Sinkiang Border	41.3N	79.3E	4.9	P	44.8	83.3
20	06/06/71	Eastern Kazakh SSR	49.9N	77.8E	5.5	P	37.8	75.5
21	05/22/71	Tibet	32.4N	92.1E	5.6	P	58.1	79.8
22	05/03/71	Mindanao, Philippine Is.	8.7N	124.1E		P	93.4	65.3
23	06/28/71	Northern China	39.9N	106.2E	5.2	P	58.4	63.8
24	06/06/71	Sea of Japan	40.8N	133.3E	4.5	P	68.3	43.5
25	06/29/71	Kurile Islands	45.3N	151.7E	4.8	P	69.4	28.3
26	05/22/71	South of Kermadec Is.	33.1S	179.2W		PKP	151.5	17.6
27	06/11/71	Off East Coast Kamchatka	51.4N	159.3E	4.8	P	65.1	21.1
	11/03/71	-"-	52.3N	159.1E	4.9	P	64.4	21.0
	11/24/71	-"-	52.9N	159.2E	6.3	P	63.8	20.7
	05/27/72	Kamchatka	54.9N	156.3E	5.7	P	61.3	21.9
28	09/27/71	Novaya Zemlya	73.4N	55.1E	6.4	P	20.6	34.7
29	07/25/71	Near Islands, Aleutians	52.1N	173.1E	5.8	P	66.4	11.8

TABLE 3.1

Events used in the NORSAR location calibrations and time delay corrections. The epicenter location is based on the NOAA solution.

Table 3.1 (cont.)

Node	Event Date	Region	Lat	Lon	m_b	Phase	Dist	Azi
30	06/10/71	Fox Islands, Aleutians	52.2N	170.6W	5.3	P	67.1	1.0
31	03/15/71	Hokkaido, Japan Region	41.7N	143.7E	5.4	P	70.7	35.5
32	04/15/71	Eastern Gulf of Aden	12.9N	48.5E	5.0	P	55.2	133.4
33	07/29/71	Northern Italy	44.7N	10.2E	4.3	P	16.1	181.6
34	03/15/71	New Hebrides Is.	15.5S	167.6E	5.4	PKP	131.7	30.4
35	07/02/71	Morocco	34.1N	5.2W	4.6	P	28.7	208.5
36	07/09/71	Near Coast of C.Chile	32.5S	71.1W	6.6	PKP	114.2	246.6
	11/28/71	Chile-Argentina Border	29.8S	69.5W	5.9	PKP	111.1	246.6
	02/09/72	Near Coast of S. Chile	51.8S	74.0W	5.5	PKP	131.0	235.0
37	07/08/71	Southern Nevada	37.1N	116.1W	5.5	P	73.1	318.2
38	03/26/71	Southeastern Alaska	60.3N	141.0W	5.5	P	60.3	343.8
39	03/15/71	New Hebrides Island	15.5S	167.6E	5.4	SKP	131.7	30.4
40	04/12/71	Southern Iran	28.3N	55.6E	6.0	P	44.1	116.8
41	03/23/71	Ural Mountains Region	61.3N	56.5E	5.6	P	21.7	68.6
42	05/22/71	Turkey	38.8N	40.5E	6.0	P	28.7	126.5
43	07/27/71	Peru-Ecuador Border Reg.	2.7S	72.4W	6.3	P	89.1	262.9
	09/09/71	Near West Coast Colombia	2.3N	78.9W	4.8	P	87.9	270.9
	02/09/72	South of Panama	4.9N	82.4W	4.9	P	87.3	275.3
44	09/30/71	South Atlantic Ocean	0.5S	4.8W	6.0	P	62.4	197.7
45	08/08/71	Kermadec Islands	30.6S	178.1W	5.2	PKP	149.2	15.0
	02/09/72	-"-	30.5S	177.6W		PKP	149.1	14.3

Table 3.1 (cont.)

Node	Event Date	Region	Lat	Long	M_b	Phase	Dist	Azi
46	07/15/71	South of Fiji Isl.	25.2S	178.4E	5.3	PKP	143.4	18.9
47	07/26/71	New Britain Region	5.2S	152.2E	6.4	PKP	117.3	44.3
48	08/05/71	C.Mid-Atlantic Ridge	0.9S	22.1W	6.3	P	66.6	216.4
49	07/27/71	Andamon Isl. Region	13.8N	95.8E	5.4	P	75.6	87.4
50	11/06/71	Rat Islands	51.5N	179.1E	6.8	P	67.5	7.9
51	03/13/71	Vancouver Isl. Region	50.6N	130.0W	5.7	P	64.4	333.6
52	11/26/71	Eastern Greenland	79.4N	17.8W	5.2	P	20.5	345.4
53	09/27/71	South of Fiji Islands	25.3S	177.2W	4.7	PKP	144.0	12.5
	10/08/71	-"-	25.9S	177.2W	4.8	PKP	144.7	12.7
	12/08/71	-"-	25.4S	177.3W	5.1	PKP	144.1	12.6
54	09/12/71	South of Fiji Islands	26.7S	177.1W	5.8	PKP	145.5	12.6
55	01/15/72	Tonga Islands	18.3S	174.6W	5.6	SKP	137.3	7.7
56	11/11/71	South of Fiji Islands	25.5S	179.9E	5.1	PKP	143.9	16.9
	01/01/72	-"-	25.6S	179.6E	5.0	PKP	144.0	17.4
	03/30/72	-"-	25.8S	179.7E	4.7	PKP	144.2	17.3
57	01/02/72	South of Fiji Islands	24.9S	180.0W	4.5	PKP	143.3	16.6
	02/19/72	-"-	25.3S	179.6E	4.6	PKP	143.6	17.3
	02/25/72	-"-	25.1S	179.7W	5.2	PKP	143.5	16.3
58	09/01/71	New Hebrides Islands	14.6S	167.2E	4.6	SKP	130.8	30.8
59	09/25/71	East New Guinea Region	6.5S	146.6E	6.3	PKP	116.6	50.8

Table 3.1 (cont.)

Node	Event Date	Region	Lat	Long	M_b	Phase	Dist	Azi
60	10/23/71	South Sandwich Is. Region	57.2S	25.5W	5.6	PKP	121.1	202.1
	11/23/71	-"-	55.6S	27.9W	5.1	PKP	120.0	204.2
	12/19/71	-"-	59.6S	26.1W	5.1	PKP	123.4	201.5
	01/08/72	-"-	55.8S	28.7W	6.2	PKP	120.4	204.7
	02/25/72	-"-	60.6S	25.7W	6.0	PKP	124.3	200.8
	02/25/72	-"-	60.8S	26.5W	5.3	PKP	124.6	201.2
	03/09/72	-"-	56.1S	27.5W	5.3	PKP	120.6	203.8
	04/06/72	-"-	57.9S	26.6W	5.4	PKP	121.9	202.5
61	09/08/71	Banda Sea	6.5S	120.6E	5.5	PKKP	109.8	66.5
	09/10/71	-"-	5.9S	130.6E	6.2	PKKP	109.4	66.2
62	10/28/71	Peru-Brazil Border Reg.	8.0S	74.4W	4.9	P	94.6	261.9
	01/12/72	Western Brazil	6.9S	71.8W	5.9	P	92.4	260.3
	01/21/72	-"-	6.7S	71.9W	5.6	P	92.3	260.4
63	03/20/72	Northern Peru	6.8S	76.8W	6.1	P	94.7	264.6
	03/20/72	-"-	6.6S	76.8W	5.4	P	94.6	264.7
	03/20/72	-"-	6.8S	76.8W	5.4	P	94.8	264.7
64	02/13/72	C.Mid-Atlantic Ridge	0.9N	28.4W	5.4	P	67.0	223.5
	04/11/72	-"-	0.9N	28.3W	6.0	P	66.8	223.4
65	04/08/72	C. Mid-Atlantic Ridge	8.1N	38.8W	5.4	P	64.1	236.9
66	01/05/72	C. Mid-Atlantic Ridge	3.3N	31.3W	4.9	P	65.6	227.4

Table 3.1 (cont.)

Node	Event Date	Region	Lat	Long	M_b	Phase	Dist	Azi
67	02/27/72	West of Gibraltar	34.8N	9.1W	4.7	P	29.1	215.4
68	10/15/71	C. Mid-Atlantic Ridge	7.7N	37.3W	5.0	P	63.9	235.3
69	08/03/71	North Atlantic Ridge	28.4N	39.2W	5.0	P	46.4	248.8
70	11/22/71	North Atlantic Ridge	30.2N	42.7W	5.2	P	46.5	253.7
71	02/05/72	North Atlantic Ridge	14.6N	45.1W	5.0	P	61.1	246.4
72	09/08/71	North Atlantic Ocean	53.8N	35.3W	4.9	P	25.4	274.9
	04/03/72	-"-	54.3N	35.1W	5.4	P	25.1	275.6
	04/03/72	-"-	54.3N	35.1W	5.2	P	25.0	275.7
73	11/20/71	Vancouver Island Region	48.8N	129.5W	5.5	P	66.2	332.5
74	02/20/72	Gulf of California	29.9N	113.6W	5.4	P	78.9	313.1
75	09/30/71	Virgin Islands	18.1N	64.5W	4.9	P	67.2	266.3
76	08/20/71	Off Coast of Chiapas,Mex.	13.4N	92.4W	5.8	P	84.8	287.9
	09/23/71	Near Coast of Chiapas,Mex	14.5N	93.8W	4.5	P	84.4	289.7
	03/07/72	-"-	14.6N	93.8W	4.8	P	84.3	289.7
	03/08/72	-"-	14.4N	93.9W	4.9	P	84.6	289.8
	03/08/72	-"-	14.6N	93.9W	4.9	P	84.4	289.8
77	11/25/71	Alaska Peninsula	56.4N	160.7W	5.3	P	62.9	354.7
	02/21/72	-"-	55.9N	158.3W	5.7	P	63.3	353.2
	02/24/72	-"-	55.8N	158.3W	5.3	P	63.4	353.1
	03/24/72	-"-	56.1N	157.2W	6.0	P	63.0	352.5

Table 3.1 (cont.)

Node	Event Date	Region	Lat	Long	M_b	Phase	Dist	Azi
78	02/07/72	Costa Rica	8.5N	83.9W	5.5	P	84.9	278.3
79	02/15/72	Northern Colombia	6.8N	73.0W	5.0	P	81.1	267.9
80	04/07/72	Off Coast of Oregon	42.6N	126.3W	5.6	P	71.1	328.0
81	04/07/72	Southern Alaska	60.1N	152.8W	5.1	P	58.7	350.5
82	03/10/72	Near Coast of Venezuela	10.8N	62.9W	5.2	P	72.7	261.1
84	12/26/71	Kurile Islands	43.5N	147.9E	5.2	P	70.3	31.8
	02/18/72	-"-	43.6N	147.8E	4.7	P	70.2	31.8
	05/29/72	-"-	43.5N	147.7E	4.4	P	70.3	31.9
85	01/13/72	Kurile Islands	46.8N	152.5E	5.2	P	68.3	27.3
	02/26/72	-"-	46.8N	152.6E	4.9	P	68.4	27.2
	03/25/72	-"-	48.0N	153.2E	5.8	P	67.3	26.4
	04/16/72	-"-	46.5N	152.5E	4.5	P	68.6	27.4
86	09/29/71	Off East Coast Kamchatka	55.4N	163.6E	5.0	P	62.1	17.2
	12/16/71	Near East Coast Kamchatka	55.9N	162.9E	5.0	P	61.5	17.4
	12/17/71	Off -"-	55.5N	163.9E	5.5	P	62.0	16.9
	12/29/71	Komandarsky Isl. Region	55.2N	164.5E	5.0	P	62.4	16.6
87	03/20/72	Andreanof Is.,Aleutians	51.3N	179.2W	6.0	P	67.9	6.8
88	08/04/71	Hindu Kush Region	36.4N	70.8E	5.0	P	44.5	95.1
	10/14/71	Afgahnistan-USSR Border	36.4N	71.0E	5.1	P	44.7	94.9
89	11/05/71	Andoman Islands Region	10.2N	93.0E	5.7	P	77.3	91.8

Table 3.1 (cont.)

Node	Event Date	Region	Lat	Long	M_b	Phase	Dist	Azi
90	01/02/72	Southern Sinkiang Prov.	41.8N	84.5E	5.2	P	47.0	78.8
	04/09/72	Northern -"-	42.2N	84.7E	5.9	P	46.8	78.3
	04/09/72	Southern -"-	42.0N	84.6E	4.8	P	46.9	78.5
91	08/16/71	Szechwan Prov., China	28.9N	103.7E	5.5	P	66.6	72.7
	08/16/71	-"-	28.8N	103.6E	5.4	P	66.6	72.8
	04/08/72	-"-	29.6N	101.8E	5.3	P	65.1	73.8
92	12/09/71	Northeast of Taiwan	25.6N	124.4E	5.3	P	78.6	57.6
	04/17/72	Taiwan Region	24.3N	122.5E	5.1	P	78.9	59.8
	04/21/72	-"-	24.1N	122.5E	5.1	P	79.1	59.9
93	04/25/72	Mindoro, Philippine Is.	13.5N	120.5E	5.4	P	87.6	66.4
	04/26/72	-"-	13.5N	120.6E	5.0	P	87.7	66.4
	04/26/72	-"-	13.2N	120.3E	5.1	P	87.8	66.8
	04/27/72	-"-	13.4N	120.4E	5.2	P	87.6	66.5
	05/26/72	-"-	13.3N	120.4E	5.2	P	87.7	66.6
94	10/25/71	South of Honshu, Japan	30.0N	137.1E	5.3	P	79.5	45.4
95	03/08/72	South of Honshu, Japan	33.3N	140.6E	4.9	P	77.6	41.2
96	03/02/72	South of Honshu, Japan	33.4N	140.8E	5.7	P	77.6	40.9
	03/18/72	Off E.Coast Honshu, Japan	33.5N	141.2E	5.0	P	77.7	40.7
97	04/05/72	Hokkaido, Japan Region	42.0N	142.3E	5.2	P	70.2	36.4
98	09/30/71	Eastern Siberia	61.6N	140.3E	5.4	P	51.9	28.0

Table 3.1 (cont.)

Node	Event Date	Region	Lat	Long	M_b	Phase	Dist	Azi
99	04/18/72	Lake Tanganyika Region	3.0S	28.7E	5.4	P	65.1	160.3
100	03/07/72	Burma-India Border Reg.	23.3N	94.9E	4.3	P	67.1	83.1
101	08/31/72	Central Russia	52.3N	95.4E	5.5	P	44.2	61.2
102	01/14/72	Iran-Iraq Border Region	32.8N	46.9E	5.1	P	36.5	123.6
103	01/12/72	Tadzhik-Sinkiang Border	37.7N	75.1E	5.6	P	45.6	90.2
104	02/20/72	Tibet	34.6N	80.3E	4.8	P	50.6	88.2

Also note that nodes 1-10 and 83 are just defined border points and thus are not based on observations. The calibrations and corrections for these points are zero. For events with apparent velocity less than say 10 km/sec, there is thus no reason to ask for corrections. For apparent velocity less than 8.4 km/sec, the corrections are not defined. This will be a point outside the grid shown in Fig. 3.1.

Table 3.2 lists for each node point its location in slowness space (UX,UY), its calibrated location (UCX,UCY), and the regional corrections for this node point. As mentioned above, nodes 1-10 and node 83 have no regional corrections and no calibration, which may also be seen from this table.

TABLE 3.2

Regional corrections for 104 node points implemented 30 Nov 72. UX,UY is observed and UCX,UCY corrected locations in slowness space, units ms/km. The last 22 columns give time delay corrections in milli-seconds for each of the 22 subarrays.

NODE	UX	UY	UCX	UCY	01A	01B	02B	03B	04B	05B	06B	07B	01C	02C	03C	04C	05C	06C	07C	08C	09C	10C	11C	12C	13C	14C
1	-69	120	-69	-120	0	0	0	0	0	0	0	0	0	0	0	0	0	0	0	0	0	0	0	0	0	0
2	-120	69	-120	-69	0	0	0	0	0	0	0	0	0	0	0	0	0	0	0	0	0	0	0	0	0	0
3	-120	15	-120	15	0	0	0	0	0	0	0	0	0	0	0	0	0	0	0	0	0	0	0	0	0	0
4	-120	69	-120	69	0	0	0	0	0	0	0	0	0	0	0	0	0	0	0	0	0	0	0	0	0	0
5	-69	120	-69	120	0	0	0	0	0	0	0	0	0	0	0	0	0	0	0	0	0	0	0	0	0	0
6	0	120	0	120	0	0	0	0	0	0	0	0	0	0	0	0	0	0	0	0	0	0	0	0	0	0
7	69	120	69	120	0	0	0	0	0	0	0	0	0	0	0	0	0	0	0	0	0	0	0	0	0	0
8	120	69	120	69	0	0	0	0	0	0	0	0	0	0	0	0	0	0	0	0	0	0	0	0	0	0
9	120	-69	120	-69	0	0	0	0	0	0	0	0	0	0	0	0	0	0	0	0	0	0	0	0	0	0
10	69	-120	69	-120	0	0	0	0	0	0	0	0	0	0	0	0	0	0	0	0	0	0	0	0	0	0
11	1	-27	3	-51	0	-5	207	113	-113	-40	45	14	34	162	262	252	153	30	43	209	203	262	206	284	55	64
12	42	-20	43	-18	0	-28	38	59	187	2	34	11	-206	-145	-98	8	11	120	-203	-186	-154	-98	66	65	-10	-100
13	45	-10	44	-7	0	17	40	54	162	-127	31	85	-244	-65	-185	-11	95	61	-246	-200	-200	-95	115	88	-66	-173
14	57	-1	56	0	0	36	11	34	-28	-141	107	94	-206	-103	-148	16	85	110	-261	-145	-110	-51	3	96	-91	-143
15	-72	2	-72	0	0	-3	126	110	91	-60	124	-67	59	111	452	375	443	179	68	22	215	396	406	542	278	-16
16	-41	1	-41	4	0	-51	-35	-57	108	73	163	136	-23	-31	144	194	269	67	198	57	18	-85	27	299	335	42
17	-67	-1	-66	-2	0	19	126	91	117	2	564	-14	174	201	467	563	588	223	132	19	272	465	437	578	331	54
18	-74	25	-67	25	0	-63	107	21	81	-31	225	551	-51	2	495	530	545	77	75	47	154	395	385	435	303	-21
19	-71	-6	-71	-6	0	90	247	241	206	110	188	32	155	201	462	523	485	299	228	121	208	462	581	651	351	137
20	-71	-15	-73	-13	0	25	125	41	122	22	-11	42	50	106	342	321	267	231	158	125	159	245	338	395	320	119
21	-64	-7	-61	-11	0	56	195	135	130	114	209	18	223	232	463	511	620	258	237	132	356	462	544	538	407	196
22	-45	-17	-37	-17	0	71	145	46	77	140	360	147	205	213	480	578	495	167	340	170	195	358	582	506	336	123
23	-58	-21	-55	-25	0	134	475	181	127	122	191	100	266	226	330	519	553	251	238	92	335	468	601	459	331	240
24	-43	-36	-37	-39	0	111	279	213	-48	-24	85	158	165	195	297	481	535	104	180	21	242	577	576	436	129	104
25	-30	-47	-26	-43	0	3	142	67	-117	-87	5	-48	76	160	160	313	411	-22	-76	-103	414	427	248	152	-51	4
26	-13	-21	-7	-22	0	10	-21	-91	-113	207	-14	-49	-252	-114	153	-17	-153	-155	-111	426	-49	-204	-48	-22	12	-99
27	-22	-37	-21	-34	0	117	232	213	7	76	34	-125	164	242	217	332	341	52	-118	78	525	398	270	257	82	73
28	-65	-68	-56	-61	0	101	174	176	172	-33	2	74	133	213	32	-78	43	307	502	71	59	16	92	314	175	294
29	-14	-54	-11	-56	0	180	273	223	71	76	86	59	161	242	272	350	337	156	-16	216	489	373	334	343	216	64
30	-2	-54	0	-57	0	183	230	210	20	688	130	153	215	260	321	376	358	134	69	330	323	262	275	359	280	185
31	-36	-47	-31	-44	0	95	186	151	-31	10	119	77	115	185	254	341	321	45	89	-97	162	509	420	302	31	-17
32	-57	41	-47	44	0	-176	-131	-166	-55	-38	-221	-21	-135	-140	-212	-125	-152	-204	-35	-88	-196	-213	-171	-185	-106	14
33	0	105	3	115	0	-8	145	135	108	-38	-16	83	8	176	365	151	176	221	404	-52	132	260	270	312	334	129
34	-10	-18	-8	-14	0	4	-125	-105	55	205	-85	48	-211	-22	115	-15	-181	-161	-8	-74	-130	-239	-32	31	-24	-104
35	31	74	30	73	0	-85	54	55	105	15	80	-7	100	-98	556	107	77	183	248	163	144	167	291	288	208	140
36	10	3	15	8	0	-32	117	224	86	-100	-10	90	-145	-140	-50	180	-1	85	-79	-140	-71	40	136	180	45	26
37	24	-47	35	-39	0	-9	76	73	431	-40	72	-36	165	144	294	1	-132	32	25	73	67	152	169	112	-13	-13
38	15	-60	17	-60	0	16	88	67	-77	-72	61	-17	158	209	293	134	50	-93	135	293	139	250	238	66	-32	44
39	-21	-27	-15	-25	0	-12	49	-44	-187	175	98	32	-148	-14	145	108	-24	-220	-110	-77	2	-12	62	-11	-31	-222
40	-73	31	-64	32	0	-100	14	-26	52	-28	158	352	-78	-40	415	450	452	110	27	23	128	300	322	300	335	5
41	-65	-28	-67	-34	0	54	241	230	155	253	34	34	282	166	211	275	263	324	293	212	113	241	427	327	317	261
42	-72	43	-64	47	0	-153	-68	-55	-32	-62	59	162	-159	-118	233	344	605	8	98	-199	67	180	293	379	357	-23
43	28	0	41	2	0	32	-14	-57	13	-189	-5	23	-304	-159	-159	-7	32	36	-280	-259	-161	-134	73	61	-167	-85
44	14	61	18	57	0	-147	-64	-61	-46	-82	-27	-185	163	170	102	64	144	19	354	-38	75	110	172	166	129	93
45	-13	-23	-6	-23	0	-39	-56	-144	-172	146	-112	-45	-256	-155	120	87	-255	-235	-106	-124	-142	-195	-77	72	-63	-209
46	-15	-30	-10	-30	0	-45	-7	-119	-188	155	-107	-20	-250	-97	158	100	-86	-302	-220	-30	-24	-134	41	31	-73	-253
47	-20	-17	-11	-12	0	-33	-222	-158	-12	-8	-54	-35	-212	-106	-21	-103	-156	-179	-57	-126	-268	-301	-103	-5	-78	-170
48	28	52	34	48	0	160	260	45	58	45	93	112	47	197	378	200	132	56	232	135	205	227	344	129	202	62
49	-58	-2	-51	-2	0	20	114	95	130	204	320	126	192	227	534	512	574	135	246	185	229	526	270	619	399	143
50	-10	-54	-7	-58	0	103	241	181	87	203	72	58	186	246	413	378	218	132	33	292	410	358	316	373	256	95
51	25	-54	26	-52	0	-18	80	34	-75	-122	-18	-55	135	222	234	134	-19	-67	76	167	187	249	250	26	-90	26
52	24	-53	25	-54	0	11	-25	55	53	43	128	69	33	88	118	220	66	47	-38	63	82	185	48	106	12	44
53	-11	-21	-6	-31	0	-63	-20	-91	-165	195	-133	-54	-208	-174	138	95	-62	-245	-198	-26	-46	-109	84	95	-71	-201
54	-11	-29	-7	-29	0	-85	-31	-58	-68	145	-4	-44	-221	-108	86	27	-58	-223	-111	-152	-182	-192	62	133	-70	-239
55	-8	-29	-3	-27	0	-37	-24	-64	-113	123	-161	-48	-218	-230	76	68	-110	-252	-162	-91	-156	-151	-4	95	-56	-202
56	-14	-29	-8	-27	0	-120	-70	-165	-200	160	-109	-65	-238	-169	61	3	-110	-313	-216	-91	-257	-326	54	112	-143	-283
57	-14	-31	-9	-31	0	21	4	-107	-200	134	-120	-45	-245	-111	220	103	-32	-258	-238	2	-23	-114	64	96	-102	-217
58	-23	-30	-17	-30	0	-117	85	-12	-200	189	57	3	-89	3	197	174	-17	-215	-128	-90	80	43	129	15	-41	-219
59	-21	-10	-13	-10	0	-205	-275	-352	-143	-104	-173	-160	-421	-273	-148	-273	-351	-326	-159	-352	-431	-453	-225	-184	-251	-292
60	-1	20	6	15	0	-89	102	10	-89	-254	-167	-164	-254	-105	-166	-269	-215	-81	69	-184	-278	-187	-22	49	-102	-115
61	22	12	25	10	0	61	63	158	122	-9	37	-13	-31	-35	56	43	225	226	-54	-25	87	95	173	160	141	152
62	37	8	40	6	0	193	57	27	123	48	142	167	-138	38	5	178	262	104	-116	-11	44	36	107	266	-22	84
63	37	4	40	3	0	168	74	20	75	-52	69	150	-152	-100	-78	128	171	100	-218	-126	-16	-73	182	194	-99	-18
64	34	47	39	41	0	70	209	238	-60	-37	129	30	28	93	268	225	-4	-165	158	132	132	203	234	80	108	-25
65	46	38	45	34	0	-47	159	152	34	-47	113	84	45	71	162	242	170	66	-97	42	245	254	188	90	75	55
66	40	44	42	39	0	-28	75	108	-74	-34	63	-18	-58	-72	242	115	-55	-213	38	61	221	-313	189	170	87	-164
67	38	65	46	65	0	80	78	118	59	118	140	173	154	254	494	131	14	244	301	177	252	239	352	136	223	160
68	44	39	48	33	0	-8	47	154	59	30	-9	-29	81	99	215	254	153	-15	11	-4	242	287	199	107	106	60
69	68	27	65	29	0	130	-17	-8	2	-29	64	198	-21	254	133	-48	126	77	17	-41	225	143	118	-82	-82	35
70	69	21	67	19	0	76	18	-29	-12	-118	-23	90	-146	15	49	-86	-94	61	-296	-161	77	127	-80	-19	-246	-145
71	52	27	55	24	0	67	38	105	90	45	134	382	41	176	252	185	233	229	47	104	216	270	182	137	190	63
72	64	-6	81	-7	0	-58	-155	-47	-58	-94	123	87	-84	-55	-72	-35	-79	323	-42	-239	-193	-79	-80	41	22	-137
73	24	-53	26	-51	0	46	112	-18	-74	-53	-80	-61	109	192	253	104	-64	-16	195	137	180	240	242	23	-61	32
74	34	-40	38	-33	0	-47	38	41	274	13	-53	-51	18	15	208	-30	-74	45	-100	-194	-10	108	145	123	-80	-133
75	56	3	56	3	0	32	4	49	-23	-142	174	129	-173	-91	-138	50	113	100	-234	-132	-129	-23	29	146	-157	-133
76	41	-17	42	-14	0	-38	16	33	138	-49	45	-14	-257	-168	-105	-32	31	88	-393	-285	-185	-50	99	10	-110	-190
77	5	-53	8	-59	0	9	194	255	-148	-71	98	29	70	165	273	275	208	-56	44	313	214	316	257	253	79	110
78	44	-5	44	-8	0	0	38	44	164	-174	-25	35	-274	-140	-158	-25	36	8	-373	-235	-140	-22	25	36	-139	-130
79	48	2	47	1	0	12	-132	-75	-81	-167	-47	-14	-284	-169	-115	-80	47	-17	-344	-171	-232	-182	175	36	-160	-289
80	26	-50	29	-48	0	44	84	7	-12	-181	13	-14	91	247	259	100	-138	34	101	137	171	204	218	44	-133	24
81	5	-61	10	-57	0	-23	171	278	14	-43	97	35	95	203	268	267	213	-50	38	305	204	317	275	218	83	136
82	53	8	52	8	0	35	117	10	-93	-147	42	259	-30	-132	-152	27	44	225	-208	-95	-85	-2	14	135	-146	-139
83	0	-120	0	-120	0	0	0	0	0	0	0	0	0	0	0	0	0	0	0	0	0	0	0	0	0	0
84	-33	-44	-29	-47	0	107	161	114	-128	-76	92	-17	93	131	208	255	310	9	-19	-76	232	480	295	224	-56	-13
85	-25	-49	-26	-50	0	51	150	98	-70	-64	72	-111	138	191	172	318	325	-18	-55	-25	441	414	249	217	-55	63
86	-15	-55	-17	-57	0	188	248	231	43	45	20	-167	156	241	273	295	343	33	-98	102	510	401	285	288	118	36
87	-8	-54	-6	-58	0	278	135	75	11	49	13	-50	118	170	321	308	241	80	-21	276	355	254	261	320	182	-9
88	-74	8	-70	8	0	-118	17	35	-57	-140	278	-132	-52	47	418	382	389	28	8	-175	160	233	304	473	152	-166
89	-58	0	-50	1	0	38	152	112	242	213	337	172	182	216	528	550	539	223	261	197	189	263	747	610	409	129
90	-69	-11	-68	-13	0	98	230	178	235	93	109	70	307	239	465	540	477	332	328	163	274	497	623	570	362	243
91	-59	-15	-55	-10	0	161	242	164	153	141	484	145	276	284	544	567	435	280	363	217	358	391	535	592	373	148
92	-48	-23	-42	-25	0	133	263	158	82	132	330	101	201	242	448	544	500	168	310	200	222	449	527	543	312	138
93	-48	-15	-39	-11	0	65	193	13	109	143	235	143	177	201	495	568	531	181	325	152	148	403	586	550	357	115
94	-38	-31	-32	-33	0	137	228	-82	-52	35	201	175	157	262	401	445	476	3	220	45	208	524	472	374	85	-19
95	-38	-34	-33	-37	0	88	240	158	-120	-91	165	124	98	204	347	395	386	5	120	56	169	501	484	354	25	20
96	-28	-35	-32	-35	0	168	265	240	-64	-13	225	140	164	203	367	473	414	47	114	53	222	538	501	402	62	42
97	-37	-41	-32	-44	0	32	182	157	-143	-75	112	36	110	143	318	312	342	63	54	-63	171	525	377	312	-42	-17
98	-23	-55	-31	-55	0	35	189	118	-48	-110	-82	68	74	163	161	230	275	52	-54	-222	414	459	168	156	25	-38
99	-27	58	-19	55	0	71	-8	37	184	-41	-168	-37	30	-22	-181	-154	-222	16	58	-29	-116	-125	-170	43	-79	12
100	-61	-5	-56	-6	0	-24	190	114	170	194	402	126	219	240	503	554	534	255	251	142	317	552	237	506	390	197
101	-69	-29	-63	-34	0	128	177	74	31	-13	49	79	110	159	281	434	389	134	215	114	124	513	455	270	262	161
102	-72	39	-63	42	0	-154	-57	-50	-72	-60	84	228	-185	-139	426	399	518	-91	36	-156	131	213	252	326	321	-41
103	-72	2	-70	0	0	21	142	178	132	-3	139	-7	140	189	572	508	971	225	122	194	350	447	452	618	327	123
104	-70	0	-67	-2	0	24	131	170	132	26	203	23	147	182	512	411	500	250	151	142	204	450	499	619	311	79

3.2 Location Calibrations

Fig. 3.2 shows the NORSAR location calibration vectors plotted in slowness space. The tail of the vector is the point where the event(s) have been observed, while the head of the arrow gives the theoretical point (the NOAA solution). Fig. 3.3 shows the azimuth effect of the vectors as a function of azimuth. That is, the vertical axis gives observed minus theoretical azimuth, while the horizontal axis is theoretical azimuth. Fig. 3.4 shows the observed slowness minus theoretical values as a function of azimuth. Analysis of other types of data indicates that the Moho interface in this area is not horizontal (Kanestrøm (1971)). The simplest possible model is therefore to try an interface which is a dipping plane. The calibrations based on P-observations have been grouped and averaged in intervals with 10 degrees spacing in azimuth. Assuming a velocity contrast of 6.6/8.2 (Kanestrøm (1971)) the dipping plane which gives the minimum squared difference between observed and predicted calibration vectors has been found. The predicted calibration vectors, that is, the calibration vectors caused by a specified dipping plane, were calculated by using the formulae developed by Niazi (1966). However, note that on p. 494 in Niazi's paper cos(r') should be replaced by -cos(r') once in eq. 6 and two times in eq. 7 (in the equation for n and the equation for m). The plane found has an upward dip direction 94 degrees clockwise from north, and the dip angle is 6 degrees. With another velocity contrast, this angle would of course change. (A contrast of 6.2/8.2 gives for example a dip angle of 4 degrees.) This model with a dipping plane somewhere in the upper mantle or at the crust-mantle interface is able to explain 36 per cent of the observed squared calibrations. That is, after the calibration effect of this plane is included, the mean square length of the location calibration vectors has been reduced with 36 per cent. On Figs. 3.3 and 3.4 the smooth curve shows the calibration effect of this minimum square error plane as a function of azimuth for events with epicenter distance 60 degrees from NORSAR.

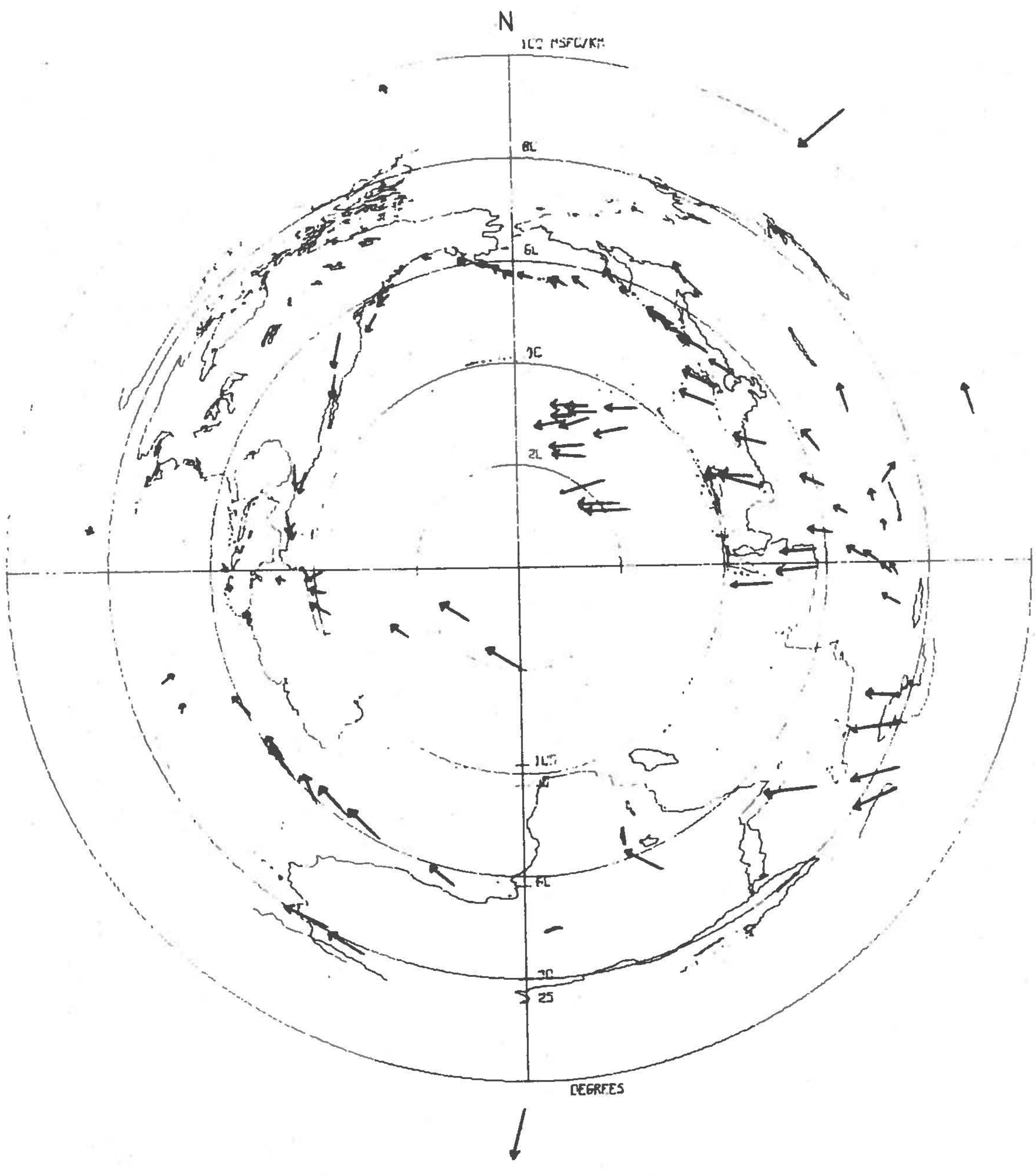

Fig. 3.2 Location calibration vectors plotted in slowness space. The tail of the arrow represents the observed point, while the head represents the NOAA solution.

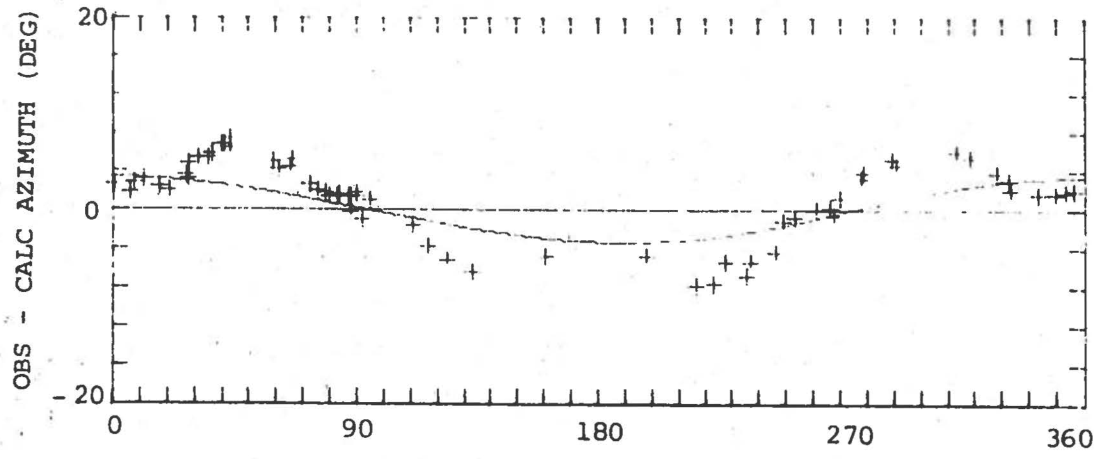

Fig. 3.3 Observed minus calculated (NOAA) azimuth as a function of calculated azimuth. The smooth curve represents the azimuth calibration effect of the dipping plane which best fits the data.

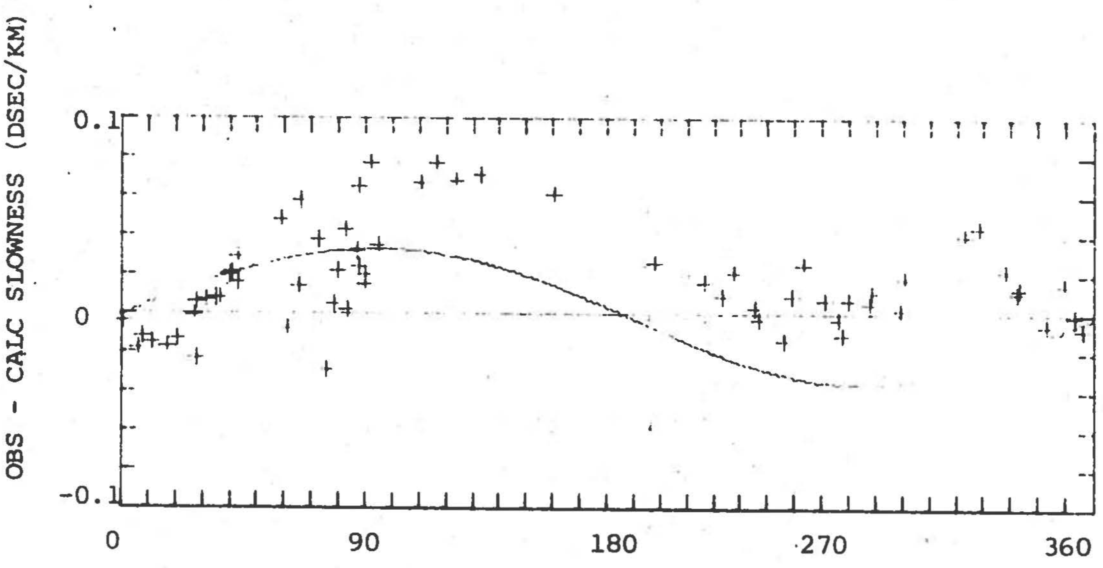

Fig. 3.4 Observed minus calculated (NOAA) slowness as a function of calculated azimuth. The smooth curve represents the slowness calibration effect of the dipping plane which best fits the data.

3.3 Time Delay Corrections

The observed regional corrections for the 22 subarrays are plotted as a function of theoretical azimuth in Fig. 3.5. For each node point the average of the corrections and the effect of elevation differences have been removed. In Fig. 3.5 only data corresponding to P-phases has been included.

The most striking feature in Fig. 3.5 is that the corrections vary relatively slowly with azimuth. From Fig. 3.2 it is seen that the P-phase data is mostly confined to a relatively narrow velocity range; it is therefore difficult to get an estimate of how much the corrections vary with slowness. However, in the azimuth interval from 45° to 100° there is also some coverage in slowness. From Fig. 3.5 it occurs that also in this azimuth interval there is relatively little variation in the data with slowness. The only clear exception from this is subarray 06B, where some of the P-phases have the same deviations as core phases. Fig. 3.6 contains all the data in Fig. 3.5, plus the data for core phases. For the subarrays 01A, 05B, 05C 09C, and 10C the core phase data are markedly different from the P-phase data, while for the rest of the subarrays there is no clear difference between the two data sets. The conclusion is thus that the deviations have a clear variation with azimuth, and that they at six subarrays also exhibit some variation with slowness.

Travel time residuals for ordinary stations are commonly approximated with the equation (Bolt and Nuttli (1966), Lilwall and Douglas(1969), Payo (1971))

$$T_{RESID} = A + B \cdot \sin(\sigma+\phi) \qquad (3.1)$$

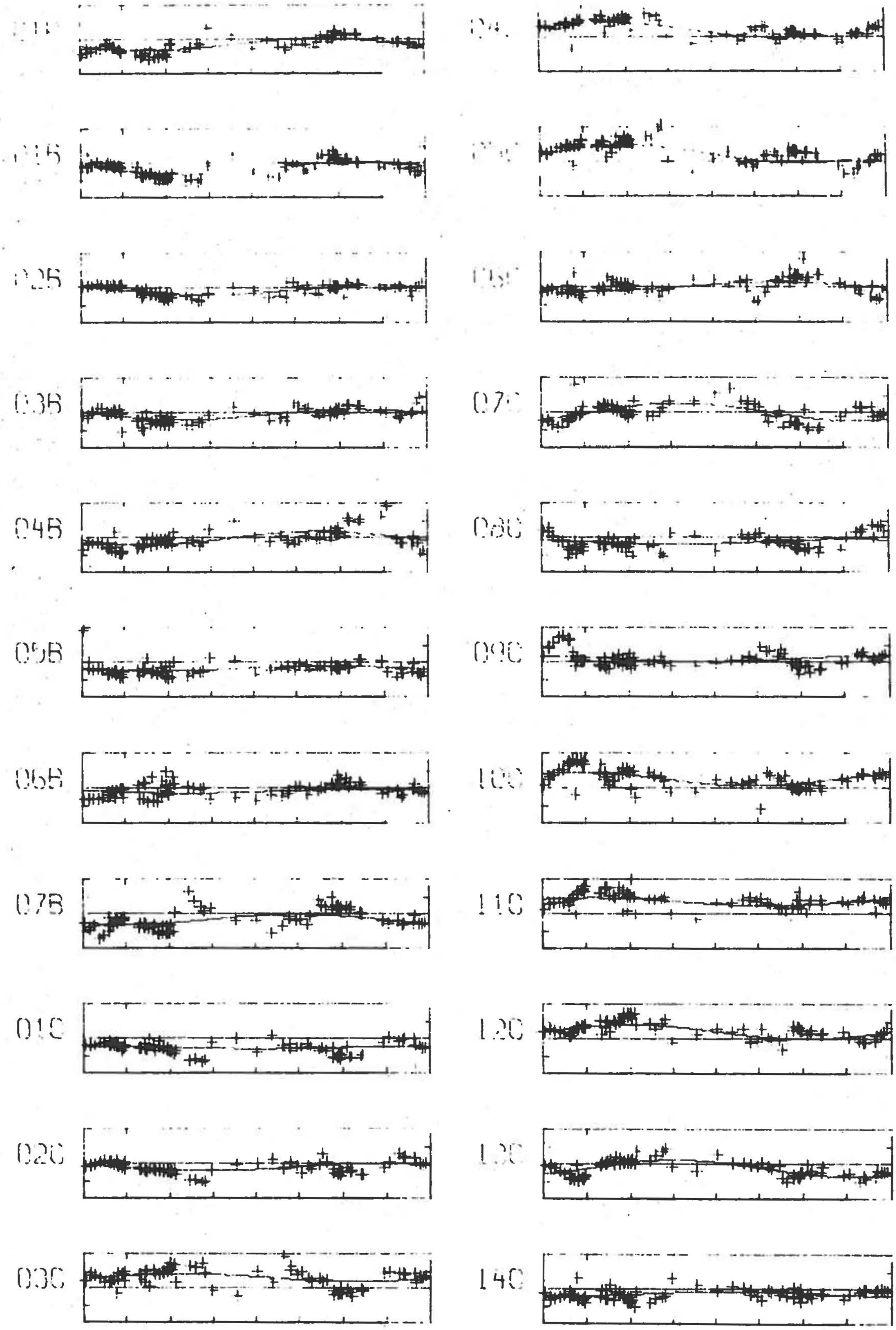

Fig. 3.5 Observed regional corrections as a function of theoretical (NOAA) azimuth. Only P-phase data has been used. The vertical axis goes from -0.5 to +0.5 seconds, while the horizontal axis goes from 0 to 360 degrees azimuth. The smooth curve represents the best fit to eq. (3.1).

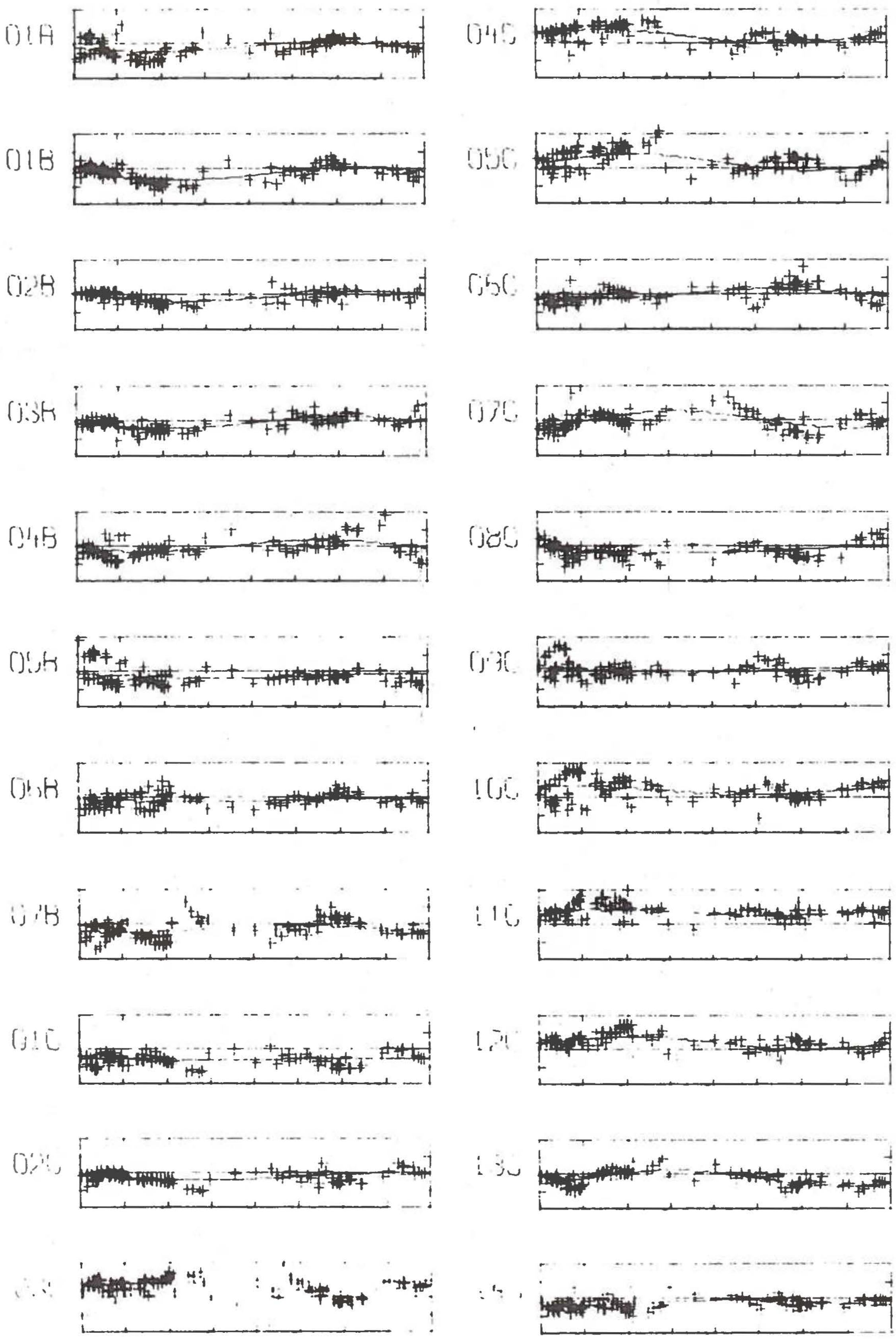

Fig. 3.6 Observed regional corrections as a function of theoretical (NOAA) azimuth. All data are used. The vertical axis goes from -0.5 to +0.5 seconds, while the horizontal axis goes from 0 to 360 degrees in azimuth. The smooth curve represents the best fit to eq. (3.1).

where σ is station azimuth and the 'early direction' is $(3/4\ \pi-\phi)$. This has been done also for the NORSAR regional corrections. The difference from the more common situation is of course that we here are talking of residuals between stations instead of absolute travel time residuals. On Fig. 3.5 and Fig. 3.6 the smooth curve is the least squares approximation of the data to equation 3.1. Before performing the approximation, the data was grouped and averaged in intervals of 10 degrees in azimuth in order to avoid that the cluster of data between 0 and 90 degrees in azimuth should have too much influence.

The values obtained for A, B and the 'early direction' are listed in Table 3.3 for the case where only P-phase data have been used. In the table are also listed the percentage reduction in mean square deviations by just subtracting the mean, corresponding to using only A in eq. 3.1 (Model 1). The next columns (Model 2) give the percentage reduction in mean square deviations by using the whole equation 3.1. As an average it is seen that A in eq. 3.1 can account for 33.6 per cent of the squared deviations, while using the whole equation 3.1 one can account for 52.2 per cent as a mean.

As will be seen, this model (2) is the one which best fits the data. For single stations there are several ways to interpret such a model (Nuttli and Bolt (1969), Lilwall and Douglas (1969), Payo (1971)). In this case with 22 stations so close together it is difficult to invert the mathematical model into physically reliable structures. For each single subarray the deviations could for example be interpreted as being caused by a plane dipping interface with depth, dip and updip direction given from A, B,

TABLE 3.3

A,B and early direction for each subarray (see eq. 3.1). Only P-phase data used. Model 1 gives reduction in mean square deviations by using only A, that is, by just subtracting the normalized mean deviations for each subarray. Model 2 gives reduction mean square deviations by using the whole eq. 3.1.

Sub No.	Name	A	B	Early Direction	Model 1 Improvement (%)	Model 2 Improvement (%)
1	01A	-0.075	0.089 ±0.031	72 ±22	34.2	60.2
2	01B	-0.076	0.094 ±0.030	112 ±20	35.1	60.2
3	02B	-0.032	0.068 ±0.017	134 ±18	18.6	55.4
4	03B	-0.026	0.077 ±0.025	108 ±20	9.0	46.1
5	04B	-0.007	0.099 ±0.040	69 ±25	0.2	27.8
6	05B	-0.094	0.037 ±0.021	78 ±36	58.7	63.5
7	06B	-0.046	0.029 ±0.020	109 ±44	26.4	31.2
8	07B	-0.083	0.075 ±0.036	44 ±30	28.9	41.8
9	01C	-0.131	0.020 ±0.023	179 ±64	69.5	70.3
10	02C	-0.051	0.058 ±0.023	132 ±25	24.3	38.4
11	03C	0.150	0.055 ±0.031	284 ±35	58.4	62.1
12	04C	0.103	0.115 ±0.019	251 ±11	46.7	75.1
13	05C	0.104	0.131 ±0.031	271 ±14	32.1	58.1
14	06C	0.008	0.064 ±0.028	68 ±27	0.7	23.7
15	07C	0.004	0.126 ±0.039	326 ±20	0.1	33.1
16	08C	-0.064	0.038 ±0.026	141 ±43	27.0	31.4
17	09C	0.042	0.049 ±0.027	171 ±34	13.4	21.0
18	10C	0.127	0.095 ±0.021	218 ±14	57.0	74.4
19	11C	0.174	0.057 ±0.020	234 ±23	79.0	83.6
20	12C	0.099	0.101 ±0.020	273 ±12	46.1	70.5
21	13C	-0.061	0.119 ±0.028	228 ±15	24.6	64.8
22	14C	-0.066	0.036 ±0.019	20 ±32	48.0	55.5
Average					33.6 ±22.4	52.2 ±18.5

and the 'early direction' (eq. 3.1). However, it is quite impossible to combine these planes in a way such that all the 22 equations (3.1) could be satisfied. In Section 5 this point will be considered further by introducing a curved interface.

In Fig. 3.7 is shown a histogram of the deviations presented in Fig. 3.6. There is a skewness in the distributions and a test for normality also shows that this data cannot be accepted as having a normal distribution (at a 0.05 level).

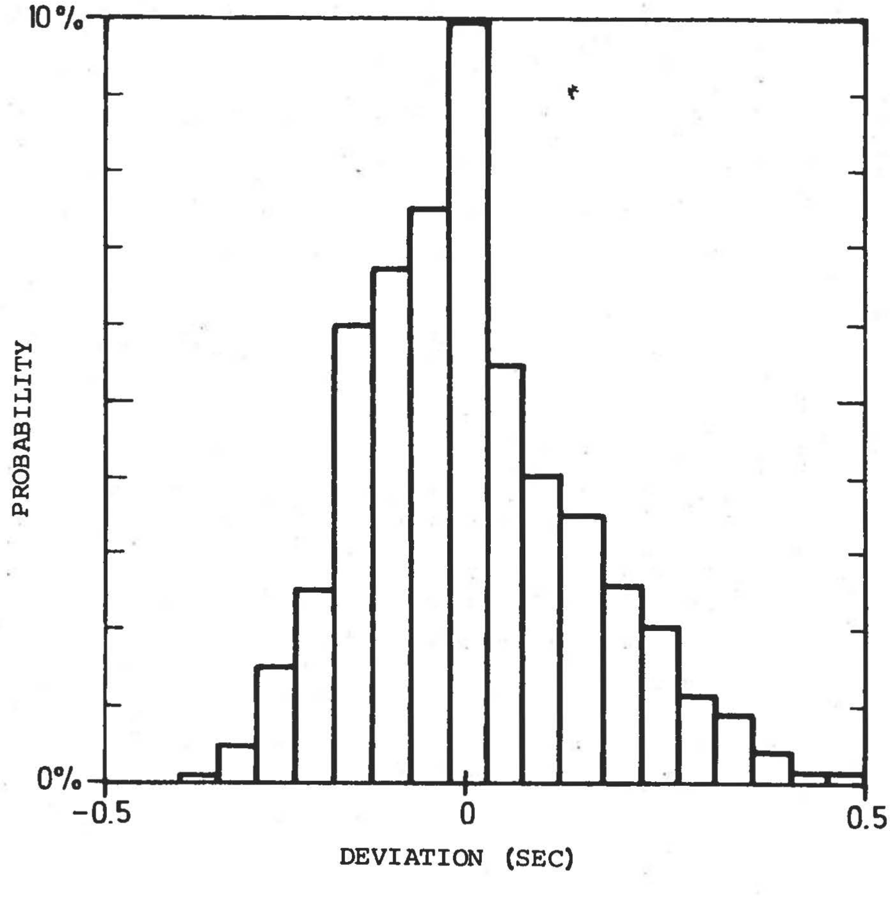

Fig. 3.7 Histogram of deviations.

4 NORSAR EVENT LOCATION AND DETECTION CAPABILITIES

4.1 Mislocation

From the foregoing data presentation it is obvious that the calibrations do have a profound influence on the location capability of the array. In order to get an estimate of this, the following procedure has been applied. For the part of the data based on P-phases the head and the tail of the arrows shown in Fig. 3.2 have been converted into real latitude and longitude, assuming epicenter depth of 33 kilometers. The distance between the two points is then calculated, and the cumulative distribution is finally found. This is presented in Fig. 4.1. Because of the skew data distribution, the average is of little interest. However, from Fig. 4.1 it is seen that for P-phases 10 per cent of the calibrations are less than 150 km, 10 per cent are greater than 1100 km and the median is 450 km. For the period from April 1972 until March 1973 Bungum and Husebye (1974) have reported a median location difference between NOAA and NORSAR epicenter solutions of 145 km for P-phases, while the 90% level was 490 km. It should here also be noted that until 30 November 1972, the old correction base was in use. The effect of the calibration vectors is thus quite obvious. The regions where NORSAR had the worst location performance were according to their paper Central America and Mid-Atlantic Ridge, which both were supplemented with several new nodes, so especially for these regions a better performance is expected in 1973.

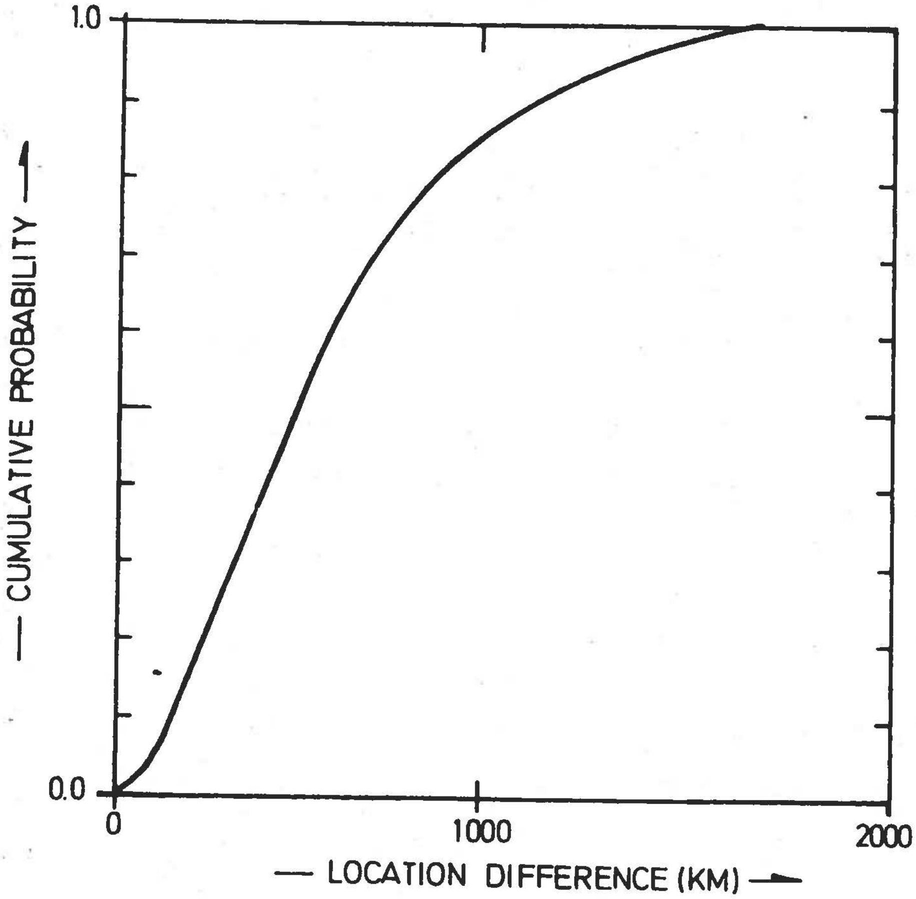

Fig. 4.1 Cumulative distribution of the length of the location calibration vectors transformed into real space. Only P-phase data are used.

4.2 SNR Gain

The array's event detection capabilities depend critically on the quality of the steering delay data used in the beamforming process. The loss in array beam gain due to erroneous time delays is frequency dependent and can be expressed as (Steinberg 1965):

$$\text{Loss(in dB)} = 170\ (\sigma/\tau)^2 \qquad (4.1)$$

where σ is the standard deviation in the time delay measurements, and τ is the dominant signal period. For P-phases Bungum and Husebye (1974) found a mean value of τ equal to 0.83 seconds. The standard deviation of the region corrections is 0.147 seconds. If these numbers are used in the equation (4.1), we find that the expected loss when no region corrections are used in beamforming is 5.3 dB.

The SNR gain from applying region corrections and calibrations has been calculated by analyzing 479 events randomly selected in the period November 1972 until September 1973. In the first case the procedure was to measure the difference in SNR between the beam this particular event was detected on (in the Detection Processor (DP)) and the beam DP would have used if no regional corrections had been available. The filter applied was the same as that used in DP in this period (1.2-3.2 Hz bandpass). The results for these calculations are presented in Fig. 4.2, Curve I. From this it is seen that without regional corrections 10% of the events would have a loss of 0.7 dB or less in DP while 10% would have a loss of 9.5 dB or more. This first number is only partially real, since the procedure applied necessarily implies that some noise detections have been included. It is therefore likely that the values given here is somewhat conservative and that therefore less than 5% of the events actually have

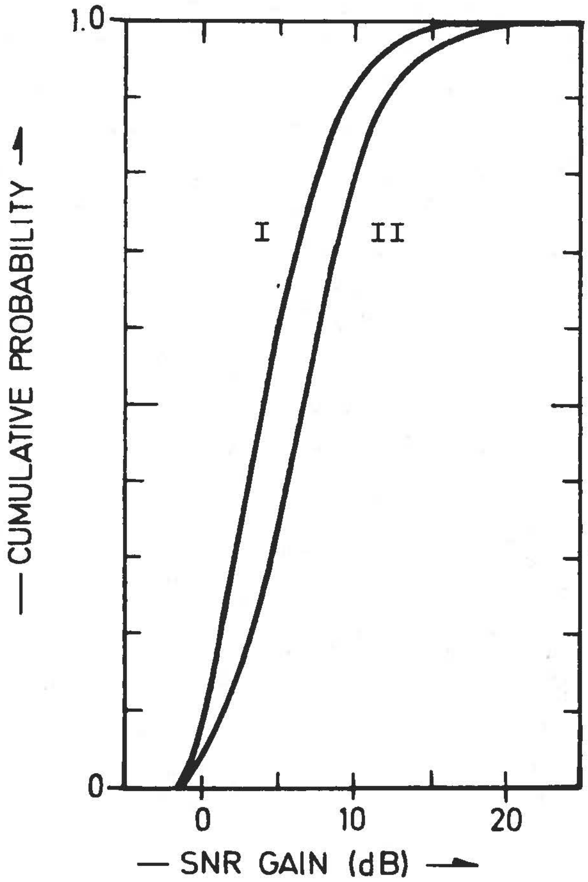

Fig. 4.2 Cumulative distribution of signal-to-noise (SNR) gain in DP. Curve I is for region corrections only, while Curve II gives the gain distribution when both region corrections and calibrations are applied.

a gain in SNR if no corrections were used. The median of the data set is 4.5 dB while the mean value is 5.2 dB. From formula 4.1 the theoretically expected value was 5.3 dB. From the considerations above, it is likely that the value of 5.2 dB should be moved somewhat upwards. The conclusion which can be drawn from this is that the corrections introduced are close to optimal. This of course does not mean that new nodes would be of no use.

The difference in SNR between the original DP beam and the beam DP would have used if neither calibrations nor region corrections had been available has also been measured. The distribution for this is plotted in Curve II, Fig. 4.2. In this case it is seen that 10% of the events would have a loss of 1.5 dB or less, while 10% of the events would have a loss of 12.5 dB or more. The median for this distribution is 6.8 dB, while the mean is 7.4 dB. The mean SNR gain by applying only regional corrections was 5.2 dB. The location calibrations thus seem to give an SNR gain which in mean is 2.2 dB.

The mean length of the calibration vectors is 0.005 sec/km. From the response pattern of the array a mis-steering of 0.005 sec/km in slowness space is expected to imply a beam loss of approximately 3 dB when measured from the peak response and assuming a signal period of 0.83 seconds. The observed mean value of 2.2 dB thus at least quantitatively indicates that the calibrations behave fairly satisfactorily with regard to SNR improvement.

5 A POSSIBLE LEAST-SQUARES INTERFACE

5.1 Introduction

As mentioned in Chapter 1, several hypotheses have been put forward in order to explain the types of deviations described here. Mainly they have been interpreted as the single or combined effect of lateral inhomogeneities at three different locations along the ray path. One, bending of the ray at the source side of the path, explained as the effect of down-dipping tectonic plates, two, bending of the ray at its deepest (turning) point, and three, inhomogeneities in the crust and upper mantle at the receiver side of the ray path. These last inhomogeneities have usually been interpreted as a Moho interface which deviates from the horizontal plane. More recently scattering caused by small random variations in the index of refraction have been found to be able to explain a large part of the anomalies observed at LASA (Aki 1973, Capon 1974). Such studies have also been performed at NORSAR (Capon and Berteussen 1973), where the conclusion so far is that the scattering in the upper mantle and crust under NORSAR is too strong to be explained by the Chernov theory (Chernov 1960). Further studies on this subject are in progress (Dahle et al 1974).

As mentioned before, the mantle-crust interface has been found to exhibit considerable variations in this area (Kanestrøm 1971). An experiment will therefore be made in order to find out how much of the deviations that possibly can be explained by a depth varying interface located somewhare in the crust or upper mantle beneath NORSAR. To be more specific, this interface will be given a reference depth of 33 km and the P-velocities below and above this interface are set to 8.2 and 6.6 km/sec respectively. The aim is then to find the curved interface which can explain as much as possible of the deviations which are observed.

5.2 Data

For this study we will recompute our region corrections so they give deviations relative to the predicted NOAA wavefront, that is:

$$DEV_{NOAA}(I) = -(UX_{NOAA}-UX_{PWF}) \cdot X(I) \qquad (5.1)$$

$$-(UY_{NOAA}-UY_{PWF}) \cdot Y(I)$$

$$+ DEV(I)$$

$DEV_{NOAA}(I)$ is the deviation for subarray I relative to the NOAA wavefront for the particular node considered, and the rest of the symbols should be self-explanatory. The part of these deviations which were from P-waves were then averaged in intervals of 10 degrees in azimuth. Fig. 51. shows the average of this data (the contours drawn). The arrows give the 'early direction', calculated as in Section 3.3. The length of the arrows are proportional to the factor B in equation 3.1.

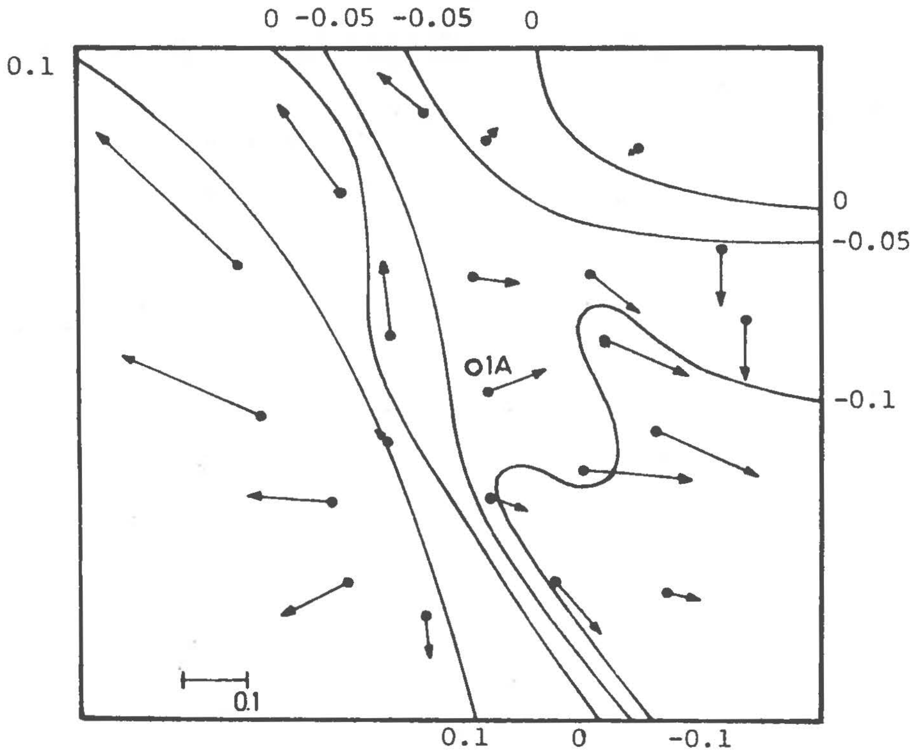

Fig. 5.1 Contours for average deviations relative NOAA wavefronts (sec) Only P-phase data has been used. The length of the arrow is proportional to B in equation 3.1 while the direction gives the early direction.

5.3 Data Analysis

In section 3.2 the dipping plane which best could explain the NORSAR calibrations was found to have an updip direction of 94° clockwise from north and a dip angle of 6° when a velocity contrast of 6.6/8.2 was assumed. This dipping plane is able to explain 17.9 per cent of the squared deviations relative to NOAA (Table 5.1). The equation for this plane may be written

$$Z = A + B \cdot X + C \cdot Y \qquad (5.2)$$

The values for A, B and C are given in row 1 on Table 5.1. Our coordinate system is then centered in the array's center with X-axis towards east, Y-axis towards north and Z-axis upwards.

Since a dipping plane cannot satisfactorily explain the deviations, we will go further and try a second degree interface. The equation for this is:

$$Z = A + BX + CY + DX^2 + EXY + FY^2 \qquad (5.3)$$

A first approximation of the coefficients A, B, ..., F are found in the following way. For each set of deviations there also is given a theoretical azimuth and apparent velocity. This makes it possible to calculate where the ray is expected to cross the horizontal Moho interface with depth equal to 33 km. The depth (Z) and (X,Y) coordinates of this point are then changed so as to make the corresponding deviation equal to zero. This procedure will give us a set of 22 points (X,Y,Z) for each of the normalized data points. Through this

TABLE 5.1

Table of coefficients for best plane, second degree interface and third degree interface. Per cent reduction in mean squared deviations is also listed for the three models.

Model	A	$B \cdot 10^3$	$C \cdot 10^3$	$D \cdot 10^3$	$E \cdot 10^3$	$F \cdot 10^3$	$G \cdot 10^6$	$H \cdot 10^6$	$I \cdot 10^6$	$J \cdot 10^6$	% Gain
Plane	-33.0	90.4	22								17.9
2nd degree	-33.4	99.3	-7.9	0.47	-2.0	0.3					21.4
3rd degree	-33.3	222.9	13.1	0.003	-1.55	0.17	33.	-13.5	-51.0	-3.9	24.3

set of points is then fitted, by the method of least squares, a second degree polynomial as described in eq. 5.3. This polynomial is our first estimate of the equation which describes the interface we are searching. When the interface can be described in this way, ray-tracing is especially simple and not very time-consuming on a computer. The next step has therefore been to vary all the coefficients in eq. 5.3 systematically. For each set of coefficients conventional ray-tracing has been applied in order to find the deviations this particular interface would give for our data points. The best interface is then the interface where the sum of the squared differences between predicted and observed deviations has been reduced to a minimum. The coefficients for this surface are listed in row 2, Table 5.1. As also can be seen from Table 5.1, this interface is able to explain only 21.4% of the squared deviations. The depth contours for this interface are plotted in Fig. 5.2.

The next step was to repeat the above procedure except that this time a polynomial of third order was used.

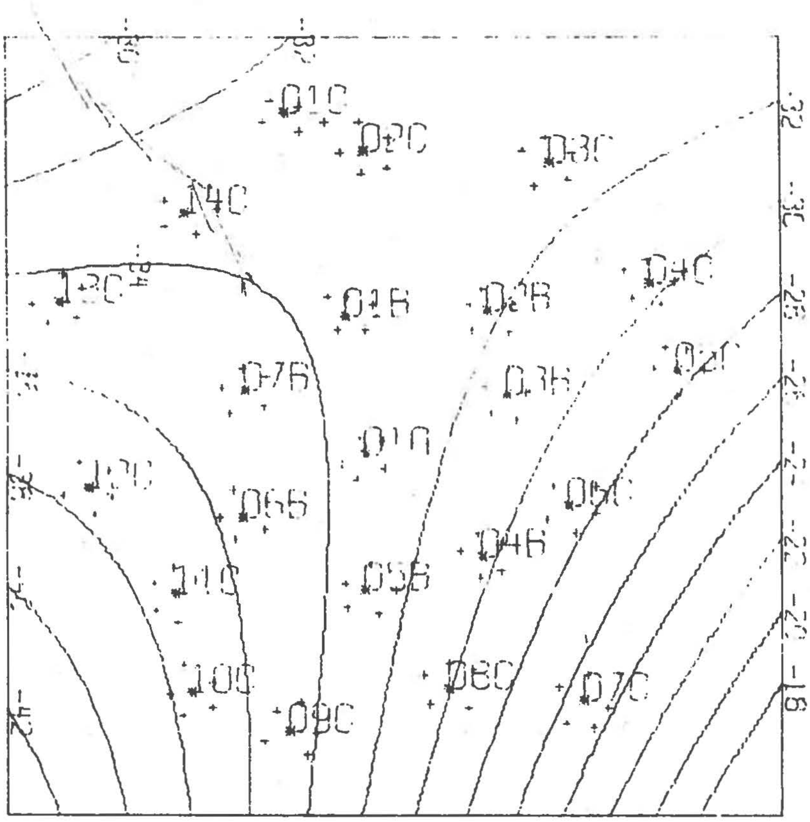

Fig. 5.2 Depth contours for best 2nd degree interface. V_C=6.6 km/sec, V_M=8.2 km/sec. The NORSAR array configuration is also included.

The equation for this is:

$$Z = A + BX + CY + DX^2 + EXY + FY^2 + GX^3 + HX^2Y + IXY^2 + JY^3 \qquad (4.4)$$

The coefficients for this interface are listed in row 3 of Table 5.1. This interface is able to explain 24.3% of the observed squared deviations. The contours for this are drawn in Fig. 5.3.

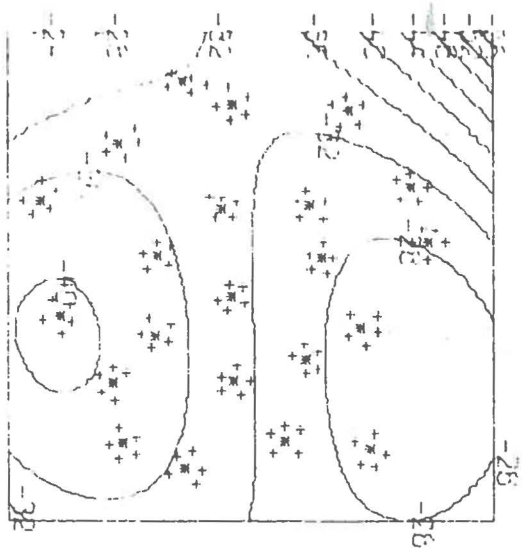

Fig. 5.3 Depth contours for best 3rd degree interface. V_C=6.6 km/sec, V_M=8.2 km/sec.

5.4 Discussion

As seen from Figs. 5.2 and 5.3, the interfaces found do exhibit such large elevation differences that their geophysical reality is questionable. To increase the order of the polynomial to higher degrees than 3 cannot be done because we then will end up with such a detailed map that simple ray theory may not be used. If the velocity in the crust above the interface is set to 6.2 km/sec, a second degree polynomial found in the same way as described in the above section will be able to explain 24.9% of the squared deviations. The contours for this interface are shown in Fig. 5.4. The conclusion is that it is not possible to construct a geophysically trustworthy interface which is able to explain more than say 25% of the sum of the squared deviations observed at NORSAR. It thus seems that in order to explain the bulk of the deviations observed, other models have to be introduced; that is, models where wave scattering and possibly multipathing take a more important part.

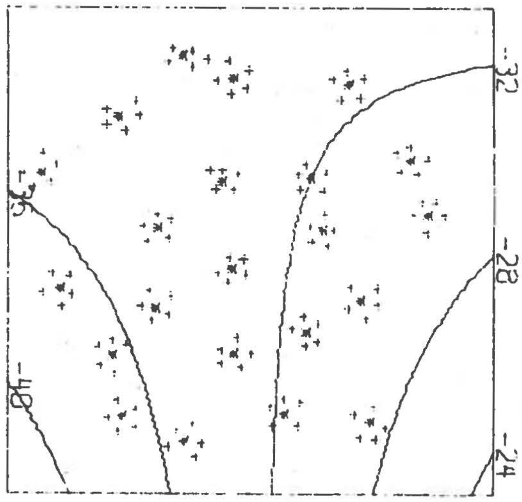

Fig. 5.4 Depth contours for best 2nd degree interface. V_C=6.2 km/sec, V_M=8.2 km/sec.

To make it quite clear, the figures 5.2, 5.3 and 5.4 are not thought of as representing a real interface. The intention with these figures and the section above is to show that the kind of deviations observed exhibits such large variations that they cannot be explained satisfactorily by any kind of relatively simple interfaces. Thus the effect of varying Moho depth cannot be dominant in this data base. In order to say something about the shape of the Moho interface, other types of data therefore have to be used (Kanestrøm 1971).

6 REFERENCES

Aki, K. (1973): Scattering of P-waves under the Montana LASA, J. Geophys. Res., 78, 1334-1346.

Bolt, B.A., and O. Nuttli (1966): P-wave residuals as a function of azimuth, I, Observations, J. Geophys. Res., 71, 5977-5985.

Bungum, H., and E.S. Husebye (1971): Errors in time delay measurements, Pure and Applied Geophys., 91, 56-70.

Bungum, H., and E.S. Husebye (1974): Analysis of the operational capabilities for detection and location of seismic events at NORSAR, Bull. Seism. Soc. Am., in press.

Capon, J. (1974): Characterization of crust and upper mantle structure under LASA as a random medium, Bull. Seism. Soc. Am., in press.

Capon, J., and K.A. Berteussen (1973): Semiannual Technical Summary Report to the Advanced Research Projects Agency, Mass. Inst. Tech., Lincoln Lab., Cambridge, Mass., USA, December 1973.

Chernov, L.A. (1960): Wave Propagation in a Random Medium, Translated by R.A. Silverman, McGraw-Hill Book Company, New York.

Chinnery, M.A., and M.N. Toksöz (1967): P-wave velocities in the mantle below 700 km, Bull. Seism. Soc. Am., 57, 199-226.

Corbishley, P.J. (1970): Multiple array measurements of the P-wave travel time derivative, Geophys. J. R. Astr. Soc., 19, 1-14.

Dahle, A., E.S. Husebye, K.A. Berteussen and A. Christoffersson (1974): Seismic wave scattering effects and velocity measurements, In preparation.

Davies, D., and R.M. Sheppard (1972): Lateral heterogeneity in the earth's mantle, Nature, 239, 318-323.

Engdahl, E.R., and C.P. Felix (1971): Nature of travel time anomalies at LASA, J. Geophys. Res., 76, 2706-2715.

Gjøystdal, H., E.S. Husebye and D. Rieber-Mohn (1973): One-array and two-array location capabilities, Bull. Seis. Soc. Am., 63, 549-569.

Glover, P., and S.S. Alexander (1969): Lateral variations in crustal structure beneath the Montana LASA, J. Geophys. Res., 74, 505-531.

Greenfield, R.J., and R.M. Sheppard (1969): The Moho depth variations under the LASA and their effect on dT/dΔ measurements, Bull. Seism. Soc. Am., 59, 409-420.

Herrin, E., et al (1968): Seismological table for P-phases, Bull. Seis. Soc. Am., 58, 1193-1241.

Husebye, E.S., R. Kanestrøm and R. Rud (1971): Observations of vertical and lateral P-velocity in the earth's mantle using the Fennoscandinavian continental array, Geophys. J. R. Astr. Soc., 26, 14-

IBM (1972): Seismic array design handbook, Federal Systems Division, International Business Machines Corporation, Gaithersburg, Maryland, USA, Chapter 7.

Iyer, H.M. (1971): Variation of apparent velocity of teleseismic P-waves across the Large Aperture Seismic Array (LASA), Montana, J. Geophys. Res., 76, 8554-8567.

Iyer, H.M.,and J.H. Healy (1972): Teleseismic residuals at the LASA USGS extended array and their interpretation in terms of crust and upper mantle structure, J. Geophys. Res., 77, 1503-1527.

Johnson, L.R. (1967): Array measurements of P velocities in the upper mantle, J. Geophys. Res., 72, 6309-6324.

Johnson, L.R. (1969): Array measurements of P velocities in the lower mantle, Bull. Seism. Soc. Am., 59, 973-1008.

Kanestrøm, R., and K. Haugland (1971): Crustal structure in southeastern Norway from seismic refraction measurements, Scientific Report 5, part 2, Seismological Observatory, University of Bergen, Norway.

Lilwall, R.C., and A. Douglas (1970): Estimation of P-wave travel times using the joint epicenter method, Geophys. J.R. Astr. Soc., 19, 165-181.

Mack, H. (1969): Nature of short-lived P-wave signal variations at LASA, J. Geophys. Res., 74, 3161-3170.

Niazi, M. (1966): Corrections to apparent azimuths and travel time gradients for a dipping Mohorovicic discontinuity, Bull. Seism. Soc. Am., 56, 491-509.

Noponen, I. (1971): Analysis of event location errors using arrays in Scandinavia, Proc. from the seminar on seismology and seismic arrays, NTNF/NORSAR, Kjeller, Norway.

Nuttli, O.W., and B.A. Bolt (1969): P-wave residuals as a function of azimuth, 2, Undulations of the mantle low-velocity layer as an explanation, J. Geophys. Res., 74, 6594-6602.

Otsuka, M. (1966): Azimuth and slowness anomalies of seismic waves measured on the central California seismographic array, Part 1, Observations, Bull. Seism. Soc. Am., 56, 223-239.

Otsuka, M. (1966a): Azimuth and slowness anomalies of seismic waves measured on the central California seismographic array, Part 2, Interpretation, Bull. Seism. Soc. Am., 56, 655-675.

Payo, G. (1971): P-wave residuals at some Iberic stations and deep structure of South-Western Europe, Geophys. J.R. Astr. Soc., 26, 481-497.

Steinberg, B. (1965): Large aperture teleseismic array theory, ARPA report of first LASA systems evaluation conference.

Zengeni, T.G. (1970): A note on azimuthal correction for dT/dΔ for a single dipping plane interface, Bull. Seism. Soc. Am., 60, 299-306.

APPENDIX 1

PROGRAM GUIDE

A subroutine SPREGC is available for those wanting to use NORSAR's corrections and calibrations. This routine has to be run on NORSAR disk N-13 (where the data is stored) and accepts the following calls.

1. Decalibration

   CALL SUDCAL(UXC,UYC,UXO,UYO)

   Input: UXC,UYC (sec/km), slowness components corresponding to theoretical (correct) event location.

   Output: UXO,UYO (sec/km), expected observed slowness components.

2. Calibration

   CALL SUCAL(UXC,UYC,UXO,UYO)

   Input: UXO,UYO (sec/km), observed slowness components.

   Output: UXC,UYC (sec/km), calibrated slowness components, to be used when transforming the observation to latitude and longitude.

3. Region Corrections

   CALL SPREGC(UX,UY,DEV)

   Input: UX,UY (sec/km), slowness components.

   Output: DEV(I), I=1,22, region corrections for subarray 1 to 22 in seconds.